Robotica (2025), **43**, pp. 4476–4497
doi:10.1017/S0263574725102968

RESEARCH ARTICLE

Modeling analysis and signal tracking experiment of a novel series–parallel stable platform system

Xinlei Xiao[1,2], Da Song[3], Lei Lu[4], Gang Li[3], Feng Xue[5] and Lixun Zhang[5]

[1]School of Automation Engineering, Northeast Electric Power University, Jilin, China
[2]School of Mechanical and Civil Engineering, JiLin Agricultural Science and Technology College, Jilin, China
[3]School of Mechanical Engineering, Northeast Electric Power University, Jilin, China
[4]Avic Chengdu Aircraft Industrial (Group) Co., Ltd., Chengdu, China
[5]College of Mechanical and Electrical Engineering, Harbin Engineering University, Harbin, China
Corresponding author: Da Song; Email: songda@neepu.edu.cn

Received: 15 June 2025; **Revised:** 8 October 2025; **Accepted:** 12 November 2025; **First published online:** 10 December 2025

Keywords: series–parallel stable platform; kinematic model; dynamic model; signal tracking; control system

Abstract

In this paper, a novel series–parallel stable platform is proposed, and its kinematic and dynamic models are established. The relationship between the length, speed, and acceleration of rolling and pitching electric push rods is analyzed. The workspace of the series–parallel stable platform is determined, and the singularity and interference are analyzed. The state-machine-based control system of the stable platform is designed. An experimental environment of the principle of the real-time control system based on dSPACE was built. A position–speed double closed-loop experiment, simulating mounting carrier of the random signal tracking, and system comprehensive performance experiment were conducted to verify the accuracy of the kinematics and dynamics model of the series–parallel stable platform and the rationality and stability of the control system.

1. Introduction

Traditional parallel platforms are usually closed mechanisms composed of static platforms, multiple kinematic chains, and rigid mobile platforms [1–3]. The closure mechanism employs multiple kinematic chains for simultaneous control, resulting in high precision and excellent stability [4–7]. The parallel platform has been widely used in aerospace, medical, and military fields owing to its high accuracy, strong real-time target-tracking ability, large bearing capacity, and compact mechanism [8–14]. The parallel platform must solve the two key problems of a large workspace and a high-precision tracking mechanism. In recent years, many scholars have achieved significant progress in the topology synthesis, kinematics, and mechanism design of parallel platforms [15–21].

Generally, the static platform of the parallel platform does not move, but the mobile platform does; therefore, its workspace is relatively small. In addition, at the edge where the kinematic chain connects the static and mobile platforms, the overall stiffness of the parallel platform is relatively small, and motion coupling occurs between multiple kinematic chains. Kinematics and dynamics modeling is complex, and singular solutions exist [22–26]. This paper proposes a novel series–parallel stable platform. The series mechanism achieves the rotation of the static platform and increases its working space. Moreover, one of the rigid hinges is supported at the center of the static and mobile platforms, which increases the overall stiffness of the stable platform.

When the parallel platform is used because there are many motion branches, the control system must process multiple branch chain motions simultaneously, and good real-time performance is difficult to achieve [27–33]. A finite automatic state machine is a mathematical model composed of finite states and events, conditions, transitions, and actions between states; it is used to express the logic of time

© The Author(s), 2025. Published by Cambridge University Press.

https://doi.org/10.1017/S0263574725102968 Published online by Cambridge University Press

sequence processing. The modeling and simulation of a complex logic system using Stateflow can visualize the entire workflow and intuitively reflect the dynamic logic relationship; the control system has a high processing speed and a relatively simple algorithm. To improve the real-time performance and signal tracking accuracy of the control system and simplify the control algorithm, this paper proposes a state-machine-based platform control system. This mechanism and system will primarily be utilized for stabilizing platforms in vehicles or ships, ensuring the horizontal stability of radar or lighting systems.

The rest of this paper is organized as follows: The second part is the design and analysis of series–parallel stable platform. In the third part, kinematics and dynamics models of the platform are established, and the accuracy of forward and inverse kinematics is verified by simulation experiments. In the fourth part, the dynamic model of the platform is established to determine the relationship between the output forces of the two push rods. In the fifth part, the singularity and interference of the platform are analyzed, and the workspace of the platform is determined. In the sixth part, the platform control system based on the state machine is established, the system workflow and experimental environment are designed, and the position speed double closed loop experiment, simulating the mounting carrier of the random signal tracking experiment and the system comprehensive performance experiment, is carried out. Finally, the conclusions are summarized in Section 7.

2. Design and analysis of series–parallel stable platform

A stable platform is designed to isolate the rolling and pitching motions of the mounting carrier, maintain the stable state of the platform load relative to the earth, and have the function of rotation. Therefore, the design of the stable platform requires three rotational degrees of freedom, corresponding to the pitch degrees of freedom of the mounting carrier rolling and pitching motions and the azimuth adjustment mechanism.

2.1. Design scheme of series–parallel stable platform

The series–parallel three-degree-of-freedom stable platform is achieved using a two-degree-of-freedom parallel platform with a passive chain that can rotate around two orthogonal axes and a pair of gear-driven azimuth mechanisms in series. The three degrees of freedom of the stable platform can be described as pitch, roll, and azimuth. The pitch and roll are designed and implemented based on a two-degree-of-freedom parallel mechanism with a passive chain, which achieves the function of isolating the mounting carrier roll and pitch motions. The azimuth motor rotates a gear drive to adjust the azimuth angle. Azimuth rotation drives the rotation of the entire parallel platform, achieving the function of azimuth adjustment according to different azimuth angles. Based on the functional requirements of practical applications, a series–parallel three-degree-of-freedom stable platform is designed herein. Its principle is shown in Figure 1, and the prototype designed according to this principle is shown in Figure 2.

2.2. Analysis of azimuth mechanism

For any point on the moving platform, its motion is the superposition of pitch and roll motion, as shown in Figure 3. Let the mounting carrier roll angle be α, the mounting carrier pitch angle be β, angle $\angle AOP = \gamma$, $\|OP\| = r$, and angle$\angle P'OP = \psi$.

The direction of the actual ψ is related to the symbol of the projection P'_z of P' in the z direction, that is, P'_z is timing, and ψ is positive; when P'_z is zero, ψ is zero; when P'_z is negative, ψ is negative. Therefore, the relationship between α, β, γ, and ψ can be obtained as

$$\begin{cases} P' = \begin{bmatrix} c\alpha & 0 & s\alpha \\ 0 & 1 & 0 \\ -s\alpha & 0 & c\alpha \end{bmatrix} \begin{bmatrix} 1 & 0 & 0 \\ 0 & c\beta & -s\beta \\ 0 & s\beta & c\beta \end{bmatrix} \begin{bmatrix} rc\gamma \\ rs\gamma \\ 0 \end{bmatrix} \\ \psi = \arccos(a+b+c)\,\mathrm{sgn}(d-e) \end{cases} \tag{1}$$

where $a = \cos^2\gamma\cos\alpha, b = \cos\gamma\sin\gamma\sin\alpha\sin\beta, \quad c = \sin^2\gamma\cos\beta, d = \sin\gamma\cos\alpha\sin\beta,$ and $e = \cos\gamma\sin\alpha$.

https://doi.org/10.1017/S0263574725102968 Published online by Cambridge University Press

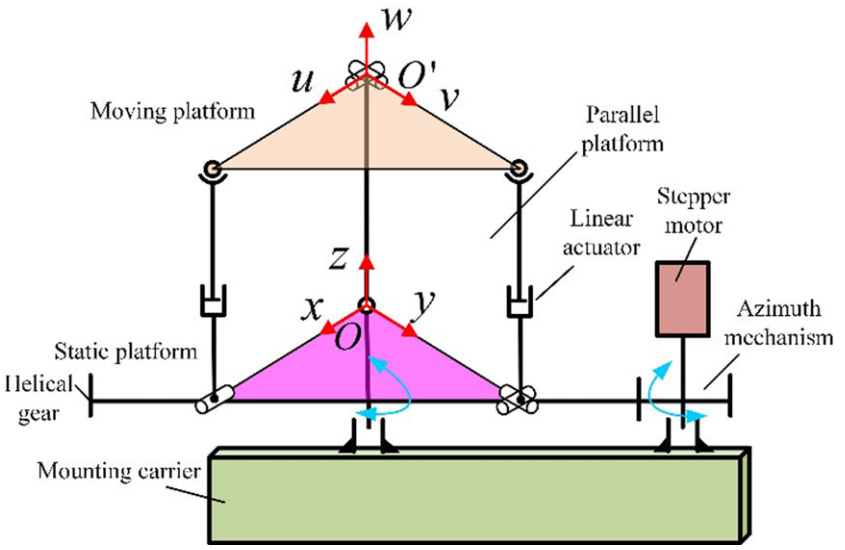


Figure 1. *Schematic of the series–parallel stable platform.*

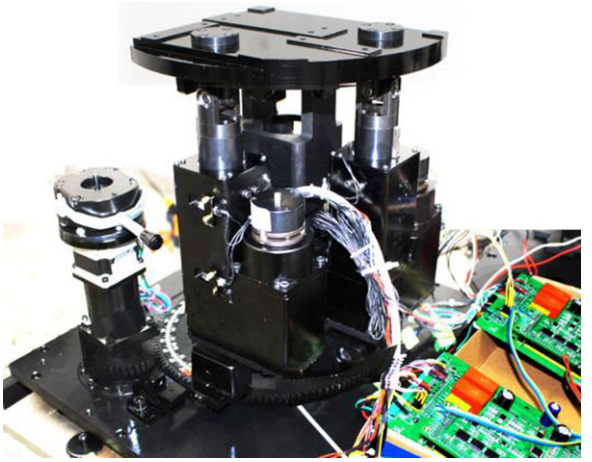


Figure 2. *The prototype of the series–parallel stable platform.*

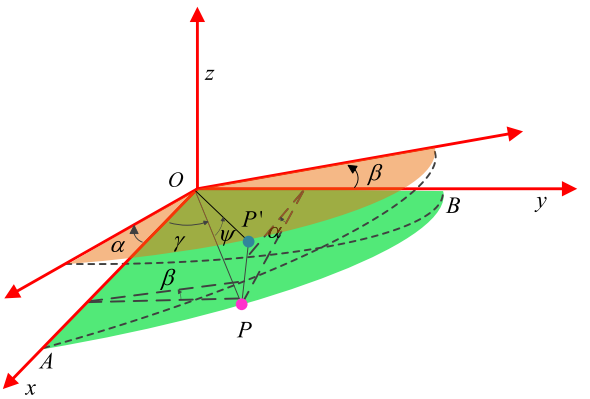


Figure 3. *Transformation of azimuth motion coordinates.*

https://doi.org/10.1017/S0263574725102968 Published online by Cambridge University Press

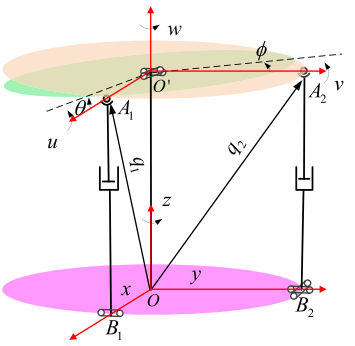


Figure 4. *Schematic of the parallel platform.*

2.3. Analysis of parallel mechanism

The parallel platform consists of branches RPS, UPS, and U of the passive chain. The center of the ball joint connecting branch RPS to the moving platform is A_1, and the center of the rotating pair connecting the branch to the lower platform is B_1. The center of the ball joint connecting branch UPS to the moving platform is A_2, and the center of the rotating pair connecting the branch to the lower platform is B_2. The coordinate system $O' - uvw$ is established on the upper platform. The origin O' is the center of the U branch of the Hooke hinge. The u axis is collinear with $O'A_1$, the v axis is collinear with $O'A_2$, and the w axis is collinear with $O'O$. The direction of each coordinate axis is shown in Figure 4. The coordinate system $O' - uvw$ is established on the lower platform. Origin O is the projection of point O' on the lower platform, the x axis is collinear with OB_1, the y axis is collinear with OB2, and the z axis is collinear with $O'O$. Coordinate system $O - xyz$ is parallel to coordinate system $O' - uvw$, and each coordinate axis point is shown in Figure 4. During analysis, $O' - uvw$ is a moving coordinate system, and $O - xyz$ is a fixed coordinate system.

Any vector q_{uvw} in $O' - uvw$ is converted to $O - xyz$ as q_{xyz} using a homogeneous transformation matrix $\boldsymbol{T}_{\text{tran}}$:

$$\boldsymbol{q}_{\text{xyz}} = \boldsymbol{T}_{\text{tran}} \cdot \boldsymbol{q}_{\text{uvw}} \tag{2}$$

where $\boldsymbol{T}_{\text{tran}}$ is

$$\boldsymbol{T}_{\text{tran}} = \begin{bmatrix} t_{11} & t_{12} & t_{13} & t_{14} \\ t_{21} & t_{22} & t_{23} & t_{24} \\ t_{31} & t_{32} & t_{33} & t_{34} \\ t_{41} & t_{42} & t_{43} & t_{44} \end{bmatrix} = \begin{bmatrix} \boldsymbol{R}_{3\times3} & \boldsymbol{P}_{3\times1} \\ \boldsymbol{O}_{1\times3} & \boldsymbol{I}_{1\times3} \end{bmatrix} \tag{3}$$

where $\boldsymbol{R}_{3\times3}$ is the rotation matrix, $\boldsymbol{P}_{3\times1}$ is the position vector matrix, $\boldsymbol{O}_{1\times3}$ is the zero matrix, and $\boldsymbol{I}_{1\times1}$ is the identity matrix.

The roll electric push rod of the parallel platform drives the moving platform to rotate around axis u (roll direction), and the pitch electric push rod drives the moving platform to rotate around axis v (pitch direction). The height of $O'O$ is set as h, the mounting carrier pitch angle as β, and the roll angle as α; the platform rotates θ around the v axis (pitch direction), ϕ around the u axis (roll direction), and γ around the w axis (azimuth direction) with the azimuth mechanism; if $c = \cos$, $s = \sin$, then the rotation matrix $\boldsymbol{R}_{3\times3}$ is

$$\boldsymbol{R}_{3\times3} = \boldsymbol{R}_{w,\gamma}\boldsymbol{R}_{v,\theta}\boldsymbol{R}_{u,\phi} = \begin{bmatrix} c\gamma c\theta & -s\gamma c\phi + c\gamma s\theta s\phi & s\gamma s\phi + c\gamma s\theta c\phi \\ s\gamma c\theta & c\gamma c\phi + s\gamma s\theta s\phi & -c\gamma s\phi + s\gamma s\theta c\phi \\ -s\theta & c\theta s\phi & c\theta c\phi \end{bmatrix} \tag{4}$$

The position vector matrix $\boldsymbol{P}_{3\times1}$ is

$$\boldsymbol{P}_{3\times1} = \begin{bmatrix} 0 & 0 & h \end{bmatrix}^T \tag{5}$$

https://doi.org/10.1017/S0263574725102968 Published online by Cambridge University Press

That is, the transfer matrix $\boldsymbol{T}_{\text{tran}}$ is

$$\boldsymbol{T}_{\text{tran}} = \begin{bmatrix} c\gamma c\theta & -s\gamma c\phi + c\gamma s\theta s\phi & s\gamma s\phi + c\gamma s\theta c\phi & 0 \\ s\gamma c\theta & c\gamma c\phi + s\gamma s\theta s\phi & -c\gamma s\phi + s\gamma s\theta c\phi & 0 \\ -s\theta & c\theta s\phi & c\theta c\phi & h \\ 0 & 0 & 0 & 1 \end{bmatrix} \tag{6}$$

3. Kinematics and dynamics modeling analysis

The kinematics of the series–parallel stable platform is divided into the following two basic problems: one is to solve the output angle of the moving platform when the telescopic displacement of the electric push rod is known, which is called the forward kinematics problem. The other is to determine the output angle of the moving platform to solve the telescopic displacement of the electric push rod, which is called the inverse kinematics problem.

3.1. Inverse kinematics model

Assume that the basic length of the electric push rod is l=h; under the moving coordinate system $O' - uvw$, the intersection point of the spherical joint and moving platform is $\boldsymbol{A}_1$, the coordinates of $\boldsymbol{A}_2$ are represented by matrix $\boldsymbol{A}$, the fixed coordinate system $O - xyz$ represents the lower platform point $\boldsymbol{B}_1$, and the coordinates of $\mathbf{B}_2$ are represented by matrix $\boldsymbol{B}$.

$$\boldsymbol{A} = \begin{bmatrix} r & 0 \\ 0 & r \\ 0 & 0 \end{bmatrix} \boldsymbol{B} = \begin{bmatrix} r & 0 \\ 0 & r \\ 0 & 0 \end{bmatrix} \tag{7}$$

The moving platform points are set as $\boldsymbol{A}_1$ and $\boldsymbol{A}_2$, which are points $A_1^{'}$ and $A_2^{'}$ after passing the motion, respectively; the coordinates of $A_2^{'}$ under the calibration system $O - xyz$ are expressed by matrix $\boldsymbol{q}$; thus, $\boldsymbol{q}$; is

$$\boldsymbol{q} = \boldsymbol{R}_{3\times3} \cdot \boldsymbol{A} + \boldsymbol{P} = \begin{bmatrix} rc\gamma c\theta & -rs\gamma c\phi + rc\gamma s\theta s\phi \\ rs\gamma c\theta & rc\gamma c\phi + s\gamma s\theta s\phi \\ h - rs\theta & h + rc\theta s\phi \end{bmatrix} \tag{8}$$

After the azimuth mechanism rotates γ, $\boldsymbol{B}_1$ and $\boldsymbol{B}_2$ are transformed into $B_1^{'}$ and $B_2^{'}$, respectively, under $O' - xyz$.

$$\boldsymbol{B}_i' = \begin{bmatrix} rc\gamma & -rs\gamma \\ rs\gamma & rc\gamma \\ 0 & 0 \end{bmatrix} \tag{9}$$

If the actual rod length $l = \|\vec{B_i'A_i'}\|$ $(i = 1, 2)$, $\vec{B_i'A_i'} = q_i - B_i'$ $(i = 1, 2)$, then $\vec{B_i'A_i'}$ is

$$\vec{B_iA_i} = \begin{bmatrix} rc\gamma(c\theta - 1) & -rs\gamma(c\phi - 1) + rc\gamma s\theta s\phi \\ rs\gamma(c\theta - 1) & rc\gamma(c\phi - 1) + s\gamma s\theta s\phi \\ h - rs\theta & h + rc\theta s\phi \end{bmatrix} \tag{10}$$

The actual rod lengths l_1 and l_2 respectively are

$$l_1 = \sqrt{[r\,(1 - c\theta)]^2 + (h - rs\theta)^2} \tag{11}$$

$$l_2 = \sqrt{(rs\theta s\phi)^2 + [r\,(1 - c\phi)]^2 + (h + rc\theta s\phi)^2} \tag{12}$$

The change in the pitch and roll electric push rod is expressed as δl_1, δl_2, $\delta l_i = l_i - l$ $(i = 1, 2)$. The relationship with the rotation angle of the parallel platform is

$$\delta l_1 = l_1 - l = \sqrt{[r\,(1 - c\theta)]^2 + (h - rs\theta)^2} - h \tag{13}$$

https://doi.org/10.1017/S0263574725102968 Published online by Cambridge University Press

$$\delta l_2 = l_2 - l = \sqrt{(rs\theta s\phi)^2 + [r\,(1 - c\phi)]^2 + (h + rc\theta s\phi)^2} - h \tag{14}$$

3.2. Forward kinematics model

For the forward kinematics of the series–parallel stable platform, the extension and contraction amount $\delta l_i = l_i - l\,(i = 1, 2)$ of the electric push rod is known, and the output value of the platform pose angle is solved, that is, pitch angle θ and roll angle φ of the parallel platform. It can be seen from Eq. (11) that the rod length l_1 is a function of pitch angle θ, independent of roll angle ϕ and azimuth angle γ. It can be obtained by simplifying the squares of both sides.

$$\frac{h}{r}s\theta + c\theta = \frac{2r^2 + h^2 - {l_1}^2}{2r^2} \tag{15}$$

Let $k_1 = \frac{h}{r}$, $w_1 = \frac{2r^2+h^2-{l_1}^2}{2r^2}$ (k1 and w1 are constants); the following is obtained:

$$k_1 s\theta + c\theta = w_1 \tag{16}$$

Let $t_1 = \tan\frac{\theta}{2}$, then $s\theta = \frac{2t_1}{1+t_1^2}$, $c\theta = \frac{1-t_1^2}{1+t_1^2}$; Eq. (16) can be simplified as

$$(w_1 + 1)\,t_1^2 - 2k_1 t_1 + w_1 - 1 = 0 \tag{17}$$

Solving Eq. (17),

$$t_1 = \frac{k_1 \pm \sqrt{k_1^2 - w_1^2 + 1}}{w_1 + 1} \tag{18}$$

t_1 has two solutions obtained from Eq. (18). When the expansion and contraction amount of electric pushrod 1 is $\delta l_1 = 0, l_1 = h, w_1 = 1$, that is, $\theta = 0, t_1 = \tan\frac{\theta}{2} = 0$, the following can be obtained

$$t_1 = \frac{k_1 - \sqrt{k_1^2 - w_1^2 + 1}}{w_1 + 1} \tag{19}$$

$$\tan\frac{\theta}{2} = \frac{k_1 - \sqrt{k_1^2 - w_1^2 + 1}}{w_1 + 1} \tag{20}$$

Therefore,

$$\theta = 2\arctan\left(\frac{k_1 - \sqrt{k_1^2 - w_1^2 + 1}}{w_1 + 1}\right) \tag{21}$$

where $l_1 = \delta l_1 + h$, and δl_1 is the telescopic displacement of electric push rod 1.

Eq. (12) indicates that the rod length l_2 is a function of θ and ϕ, independent of γ, and the squares of both sides are reduced to

$$c\phi - \frac{h}{r}c\theta s\phi = \frac{2r^2 + h^2 - {l_2}^2}{2r^2} \tag{22}$$

Let $k_2 = \frac{h}{r}c\theta$, $w_2 = \frac{2r^2+h^2-{l_2}^2}{2r^2}$ (k_2 is a function of θ, and w_1 is a constant); thus,

$$t_2 = \frac{-k_2 + \sqrt{k_2^2 - w_2^2 + 1}}{w_2 + 1} \tag{23}$$

$$\phi = 2\arctan\left(\frac{-k_2 + \sqrt{k_2^2 - w_2^2 + 1}}{w_2 + 1}\right) \tag{24}$$

where $l_2 = \delta l_2 + h$, and δl_2 is the telescopic displacement of electric push rod 2.

https://doi.org/10.1017/S0263574725102968 Published online by Cambridge University Press

3.3. Velocity and acceleration analysis

To isolate the rolling and pitching motions of the mounting carrier, the extension distance of the electric push rod should be $\delta l_i = l_i - l$ $(i = 1, 2)$ to ensure that the upper platform is horizontal with respect to the geodetic coordinate. The moving speed v_i $(i = 1, 2)$ of the electric push rod can be obtained from the derivative of the actual rod length l_i with respect to time:

$$v_i = \frac{dl_i}{dt} = \frac{dl_i}{d\theta}\frac{d\theta}{dt} + \frac{dl_i}{d\phi}\frac{d\phi}{dt} \tag{25}$$

From Eqs. (11) and (12), the velocity matrix can be obtained:

$$\begin{bmatrix} v_1 \\ v_2 \end{bmatrix} = \begin{bmatrix} \dfrac{dl_1}{dt} \\ \dfrac{dl_2}{dt} \end{bmatrix} = \begin{bmatrix} \dfrac{dl_1}{d\theta}\dfrac{d\theta}{dt} + \dfrac{dl_1}{d\phi}\dfrac{d\phi}{dt} \\ \dfrac{dl_2}{d\theta}\dfrac{d\theta}{dt} + \dfrac{dl_2}{d\phi}\dfrac{d\phi}{dt} \end{bmatrix} = \begin{bmatrix} \dfrac{dl_1}{d\theta} & \dfrac{dl_1}{d\phi} \\ \dfrac{dl_2}{d\theta} & \dfrac{dl_2}{d\phi} \end{bmatrix} \begin{bmatrix} \dfrac{d\theta}{dt} \\ \dfrac{d\phi}{dt} \end{bmatrix} \tag{26}$$

It is recorded as $\boldsymbol{v} = \boldsymbol{J}\boldsymbol{q}'$, where v is the velocity matrix of the electric push rod, $\boldsymbol{J}$ is the velocity Jacobian matrix, and $\boldsymbol{q}'$ is the motion speed matrix of the parallel platform. $\boldsymbol{J}$ is

$$\boldsymbol{J} = \begin{bmatrix} \dfrac{dl_1}{d\theta} & \dfrac{dl_1}{d\phi} \\ \dfrac{dl_2}{d\theta} & \dfrac{dl_2}{d\phi} \end{bmatrix} = \begin{bmatrix} \dfrac{1}{l_1}\left(r^2 s\theta - hrc\theta\right) & 0 \\ -\dfrac{hrs\theta s\phi}{l_2} & \dfrac{1}{l_2}\left(hrc\theta c\phi + r^2 s\phi\right) \end{bmatrix} \tag{27}$$

The moving acceleration a_i $(i = 1,2)$ of the electric push rod can be derived from the derivative of the moving speed v_i with respect to time.

$$a_i = \frac{dv_i}{dt} = \frac{dv_i}{d\theta}\frac{d\theta}{dt} + \frac{dv_i}{d\phi}\frac{d\phi}{dt} \tag{28}$$

Therefore, the acceleration matrix $\boldsymbol{a}$ is

$$\boldsymbol{a} = \frac{d\boldsymbol{J}}{dt}\boldsymbol{q}' + \boldsymbol{J}\frac{d\boldsymbol{q}'}{dt} \tag{29}$$

$$\boldsymbol{a} = \begin{bmatrix} a_1 \\ a_2 \end{bmatrix} = \boldsymbol{A}\begin{bmatrix} \dfrac{d\theta}{dt} \\ \dfrac{d\phi}{dt} \end{bmatrix} + \boldsymbol{J}\begin{bmatrix} \dfrac{d^2\theta}{dt^2} \\ \dfrac{d^2\phi}{dt^2} \end{bmatrix} \tag{30}$$

4. Dynamic modeling of series–parallel stable platform

The dynamic analysis of the series–parallel stable platform mainly studies the relationship between the motion and force of the stable platform. The dynamic characteristics of the platform can achieve structural optimization design and help to develop high-precision control methods. Therefore, dynamic modeling and simulation analysis are extremely important. In this paper, the main task of the dynamic analysis of the stable platform is to solve the change of the driving force of the electric push rod output from the motion output of the moving platform. The dynamic model of the parallel platform is established based on the Lagrangian dynamic equation.

The basic expression of the second kind of Lagrangian dynamic equation is

$$Q_i = \frac{d}{dt}\frac{\partial L}{\partial \dot{q}_i} - \frac{\partial L}{\partial q_i} \quad (i = 1, 2) \tag{31}$$

where L is a Lagrangian function, E is the system kinetic energy, U is the system potential energy, $L = E\text{-}U$, qi is the ith generalized coordinate, $\dot{q}_i$ is the first derivative of the ith generalized coordinate, and Q_i is the generalized force or generalized moment of the ith generalized coordinate.

To solve the Lagrangian function, E and U must be solved under the generalized coordinates; that is, the functional expression about $\dot{q}_i$ must be obtained. The system kinetic energy primarily includes

https://doi.org/10.1017/S0263574725102968 Published online by Cambridge University Press

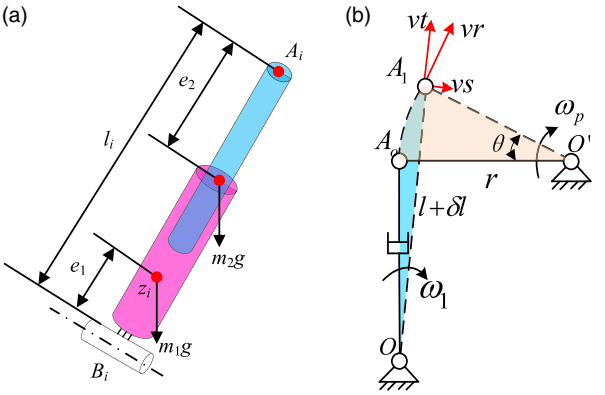


Figure 5. *Schematic diagram: (a) branch chain mechanism and (b) Rotating of moving platform.*

the kinetic energy of the cylinder block, push rod, moving platform, and stable platform load, and the system potential energy primarily includes the potential energy of the push rod and stable platform load.

Figures 5(*a*) show that the mass of the cylinder block, push rod, moving platform, and load are set as m_1, m_2, m_p, and m_f, respectively; the center of mass of the cylinder block is set as z_i; the distance from the moving pair B_i is set as e_1; the center of mass of the push rod as p_i; and the distance from the spherical hinge A_i as e_2. The generalized coordinates $\boldsymbol{q} = [\,\delta l_1 \;\; \delta l_2\,]^T$, $\dot{\boldsymbol{q}} = [\,\delta \dot{l}_1 \;\; \delta \dot{l}_2\,]^T$ are selected.

4.1. System kinetic energy

1) Kinetic energy of the cylinder block

The main movement of the cylinder block is to rotate around the rotating shaft of the rotating pair with the movement of the electric push rod, without linear movement; therefore, the rotational kinetic energy of the cylinder block when rotating around the shaft is

$$\boldsymbol{E}_1 = \frac{1}{2}\boldsymbol{\omega}_1^T \boldsymbol{I}_1 \boldsymbol{\omega}_1 \tag{32}$$

where $\boldsymbol{\omega}_1 = [\,\omega_{11} \;\; \omega_{12}\,]^T$, ω_{11} and ω_{12} are the rotational angular speeds of the cylinder blocks of branch chains 1 and 2, respectively, $\boldsymbol{I}_1 = \begin{bmatrix} \boldsymbol{I}_{11} & \\ & \boldsymbol{I}_{12} \end{bmatrix}$, $\boldsymbol{I}_{11}$ and $\boldsymbol{I}_{12}$ are the rotational inertias of the cylinder blocks, respectively, and $\boldsymbol{I}_{11} = \boldsymbol{I}_{12}$.

The rotating speed of the moving platform is shown in Figure 5(*b*). If the rotating speed of the cylinder block is w_1 and the rotating speed of the moving platform is ω_p, then $\vec{v}_r$ is

$$\vec{v}_r = \vec{v}_t + \vec{v}_s \tag{33}$$

$$\omega_p \cdot r = \omega_1 \cdot (l + \delta l) + \vec{v}_t \tag{34}$$

Because $\|\vec{v}_r\|^2 = \|\vec{v}_t\|^2 + \|\vec{v}_s\|^2$, and $\|\vec{v}_t\| = \delta \dot{l}$, then

$$\left(\dot{\theta} \cdot r\right)^2 = \left(\delta \dot{l}\right)^2 + \left(\omega_1 \,(l + \delta l)\right)^2 \tag{35}$$

Given $\dot{\boldsymbol{q}} = \boldsymbol{J} \cdot \dot{\boldsymbol{\theta}} (\dot{\boldsymbol{q}} = [\,\delta \dot{l}_1 \;\; \delta \dot{l}_2\,]^T)$;, that is, $\dot{\boldsymbol{\theta}} = \boldsymbol{J}^{-1}\dot{\boldsymbol{q}}$

$$\boldsymbol{\omega}_1 = \sqrt{\frac{\left(\dot{\boldsymbol{\theta}} \cdot r\right)^2 - \left(\delta \dot{l}\right)^2}{(l + \delta l)^2}} = \sqrt{\frac{\left(\boldsymbol{J}^{-1}\dot{\boldsymbol{q}} \cdot r\right)^2 - (\dot{q})^2}{(l + \delta l)^2}} = \frac{\sqrt{\left(\boldsymbol{J}^{-1} \cdot r\right)^2 - I_{2\times 2}}}{l + \delta l}\dot{\boldsymbol{q}} = \boldsymbol{J}_1 \dot{\boldsymbol{q}} \tag{36}$$

https://doi.org/10.1017/S0263574725102968 Published online by Cambridge University Press

Substituting Eq. (36) into $\boldsymbol{E}_1 = \frac{1}{2}\boldsymbol{\omega}_1^T \boldsymbol{I}_1 \boldsymbol{\omega}_1$,

$$\boldsymbol{E}_1 = \frac{1}{2}\boldsymbol{\omega}_1^T \boldsymbol{I}_1 \boldsymbol{\omega}_1 = \frac{1}{2}\dot{\boldsymbol{q}}^T \boldsymbol{M}_1' \dot{\boldsymbol{q}} \tag{37}$$

where $\boldsymbol{M}_1' = \boldsymbol{J}_1^T \boldsymbol{I}_1 \boldsymbol{J}_1, \boldsymbol{J}_1 = \frac{\sqrt{\left(\boldsymbol{J}^{-1} \cdot r\right)^2 - \boldsymbol{I}_{2\times 2}}}{l+\delta l}$.

2) Kinetic energy of the push rod

When the electric push rod moves, on the one hand, it moves in a straight line. On the other hand, it follows the moving platform to rotate around the rotating shaft of the rotating pair. The kinetic energy of the push rod primarily includes the kinetic energy of rotation around the axis and the kinetic energy of movement and expansion. The rotational speed of the push rod is equal to that of the cylinder block.

$$\boldsymbol{E}_2 = \frac{1}{2}\boldsymbol{v}_2{}^T \boldsymbol{M}_2 \boldsymbol{v}_2 + \frac{1}{2}\boldsymbol{\omega}_1^T \boldsymbol{I}_2 \boldsymbol{\omega}_1 \tag{38}$$

where $\boldsymbol{v}_2 = \dot{\boldsymbol{q}} = [\,\delta\dot{l}_1 \;\; \delta\dot{l}_2\,]^T$, $\delta\dot{l}_1$ and $\delta\dot{l}_2$ are the speed $\dot{l}_1$ of push rod 1 and speed $\dot{l}_2$ of push rod 2, respectively, $\boldsymbol{M}_2 = \begin{bmatrix} m_2 & \\ & m_2 \end{bmatrix}$ is the mass matrix of the electric push rod, $\boldsymbol{I}_2 = \begin{bmatrix} \boldsymbol{I}_{21} & \\ & \boldsymbol{I}_{22} \end{bmatrix}$, I_{21} and I_{22} are respectively the rotational inertia of the cylinder block, and $\boldsymbol{I}_{21} = \boldsymbol{I}_{22}$.

Substituting $\boldsymbol{v}_2 = \dot{\boldsymbol{q}}$ and $\boldsymbol{\omega}_1 = \boldsymbol{J}_1 \dot{\boldsymbol{q}}$ into Eq. (38),

$$\boldsymbol{E}_2 = \frac{1}{2}\dot{\boldsymbol{q}}^T \boldsymbol{M}' 2 \dot{\boldsymbol{q}} \tag{39}$$

where $\boldsymbol{M}_2' = \boldsymbol{M}_2 + \boldsymbol{J}_1^T \boldsymbol{I}_2 \boldsymbol{J}_1$.

3) Kinetic energy of the moving platform

The moving platform only rotates around the center of mass in the entire movement process, without translational movement; therefore,

$$\boldsymbol{E}_p = \frac{1}{2}\boldsymbol{\omega}_p^T \boldsymbol{I}_p \boldsymbol{\omega}_p \tag{40}$$

where $\boldsymbol{\omega}_1 = [\,\omega_{11} \;\; \omega_{12}\,]^T$, ω_{p1} and ω_{p2} are the angular velocities of ball joints A_1 and A_2, respectively, and $\boldsymbol{I}_p = \begin{bmatrix} \boldsymbol{I}_{p1} & \\ & \boldsymbol{I}_{p2} \end{bmatrix}$ is the moment of inertia matrix of the moving platform, $\boldsymbol{I}_{p1}$ and $\boldsymbol{I}_{p2}$ are the moments of inertia about the u and v axes, respectively.

From $\dot{\boldsymbol{q}} = \boldsymbol{J} \cdot \dot{\boldsymbol{\theta}}$ ($\dot{\boldsymbol{q}} = [\,\delta\dot{l}_1 \;\; \delta\dot{l}_2\,]^T$),

$$\boldsymbol{\omega}_p = \boldsymbol{J}^{-1}\dot{\boldsymbol{q}} \tag{41}$$

Substituting Eq. (41) into Eq. (40), we can obtain

$$\boldsymbol{E}_p = \frac{1}{2}\dot{\boldsymbol{q}}^T \boldsymbol{M}_p' \dot{\boldsymbol{q}} \tag{42}$$

where $\boldsymbol{M}_p' = (\boldsymbol{J}^{-1})^T \boldsymbol{I}_p \boldsymbol{J}^{-1}$.

4) Kinetic energy of the load

The entire platform drives the load rotate with the rotation of the moving platform. The height of the center of mass from the moving platform is h_0, as shown in Figure 6; therefore, the kinetic energy of the load is

$$\boldsymbol{E}_f = \frac{1}{2}\boldsymbol{\omega}_f{}^T \boldsymbol{I}_f \boldsymbol{\omega}_f \tag{43}$$

https://doi.org/10.1017/S0263574725102968 Published online by Cambridge University Press

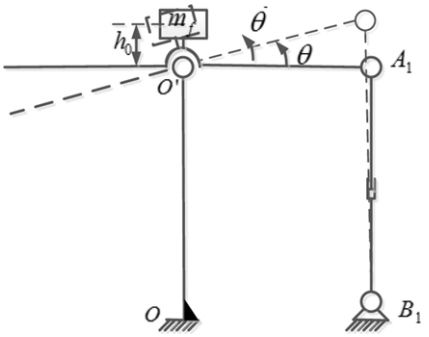


Figure 6. *Schematic of the load motion mechanism.*

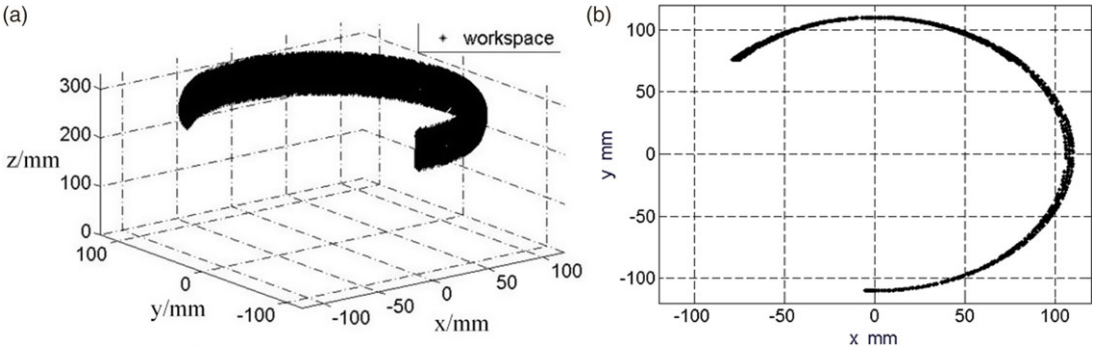


Figure 7. *Experiment on the swing platform.*

where $\boldsymbol{I}_p = \begin{bmatrix} \boldsymbol{I}_{f1} & \\ & \boldsymbol{I}_{f2} \end{bmatrix}$ is the moment of inertia matrix of the moving platform, $\boldsymbol{I}_{f1}$ and $\boldsymbol{I}_{f2}$ are the moments of inertia about the u and v axes, respectively.

Substituting $\boldsymbol{\omega}_f = \boldsymbol{J}^{-1}\dot{\boldsymbol{q}}$ into Eq. (43),

$$\boldsymbol{E}_f = \frac{1}{2}\dot{\boldsymbol{q}}^T \boldsymbol{M}_f' \dot{\boldsymbol{q}} \tag{44}$$

where $\boldsymbol{M}_f' = (\boldsymbol{J}^{-1})^T \boldsymbol{I}_f \boldsymbol{J}^{-1}$.

The total kinetic energy of the entire system is

$$\boldsymbol{E} = \boldsymbol{E}_1 + \boldsymbol{E}_2 + \boldsymbol{E}_p + \boldsymbol{E}_f = \frac{1}{2}\dot{\boldsymbol{q}}^T \left(\boldsymbol{M}_1' + \boldsymbol{M}_2' + \boldsymbol{M}_p' + \boldsymbol{M}_f'\right) \dot{\boldsymbol{q}} \tag{45}$$

4.2. System potential energy

According to the geometric relationship in Figure 6, $\angle A_1' B_1 A_1 = \angle O' B_1 A_1 - \angle O' B_1 A_1'$ can be obtained.

From the cosine theorem,

$$\angle O' B_1 A_1' = \arccos\left(\frac{\|O'B_1\|^2 + \left\|B_1 A_1'\right\|^2 - \|O'A'\|^2}{2\,\|O'B_1\| \cdot \|B_1 A_1'\|}\right) \tag{46}$$

According to the triangle characteristics of Figure 7,

$$\angle O' B_1 A_1 = \arctan\left(\frac{\|O'A_1\|}{\|A_1 B_1\|}\right) \tag{47}$$

https://doi.org/10.1017/S0263574725102968 Published online by Cambridge University Press

Thus,

$$\angle A_1' B_1 A_1 = \arctan\left(\frac{r}{h}\right) - \arccos\left(\frac{h^2 + (h+\delta l)^2}{2\cdot(h+\delta l)\cdot\sqrt{r^2+h^2}}\right) \tag{48}$$

$$\theta \approx \arccos\left(\frac{\sqrt{r^2-\delta l^2}}{r}\right) \tag{49}$$

During the expansion and contraction of the electric push rod, the cylinder block and electric push rod have certain changes in the height direction.

1) Potential energy of the cylinder block

The height of the cylinder block changes to $e_1 \cos(\alpha)$ during movement; therefore, the potential energy of the cylinder block is

$$\boldsymbol{U}_1 = m_1 g \cdot \begin{bmatrix} e_1 \cos(\alpha_1) \\ e_1 \cos(\alpha_2) \end{bmatrix} \approx m_1 g \begin{bmatrix} e_1 \\ e_1 \end{bmatrix} \tag{50}$$

2) Potential energy of the electric push rod

The extension distance of the electric push rod is δl, and the height change of the center of mass is $\delta l \cos(\alpha) \approx \delta l$; therefore,

$$\boldsymbol{U}_2 = m_2 g \begin{bmatrix} (h+q_1-e_2)\cos(\alpha_1) \\ (h+q_2-e_2)\cos(\alpha_2) \end{bmatrix} \approx m_2 g \begin{bmatrix} h+q_1-e_2 \\ h+q_2-e_2 \end{bmatrix} \tag{51}$$

3) Potential energy of the moving platform

During the movement, because the center of the moving platform is limited to a point above the center of the Hooke hinge by the column, the height does not change, but because the platform is a sector with a radius of r and an angle of 1/4 of $\pi/2$, the mass is continuously and evenly distributed; therefore, the potential energy of the moving platform changes during the movement.

According to the geometric relationship, the center of mass of the moving platform is located on the diagonal, and the distance from the center of the circle is $x = \frac{4\sqrt{2}}{3}\frac{R}{\pi}$. The height change of the center of mass is

$$\delta h = \frac{4R}{3\pi}(\sin\theta + \cos\theta \sin\phi) \tag{52}$$

The potential energy of the moving platform is

$$\boldsymbol{U}_p = m_p g \cdot \begin{bmatrix} h+\delta h_1 \\ h+\delta h_2 \end{bmatrix} \approx m_p g \begin{bmatrix} h+\frac{4}{3\pi}q_1 \\ h+\frac{4}{3\pi}q_2 \end{bmatrix} \tag{53}$$

4) Potential energy of the load

The distance between the load and center of mass of the moving platform along with the platform rotation height is $h_0 \cos(\theta)$; thus,

$$\boldsymbol{U}_f = m_f g \begin{bmatrix} h+h_0\cos(\theta) \\ h+h_0\cos(\phi) \end{bmatrix} \tag{54}$$

Substituting Eq. (49) into Eq. (54),

$$\boldsymbol{U}_f = m_f g \begin{bmatrix} h+h_0\frac{\sqrt{r^2-q_1}}{r} \\ h+h_0\frac{\sqrt{r^2-q_2}}{r} \end{bmatrix} \tag{55}$$

https://doi.org/10.1017/S0263574725102968 Published online by Cambridge University Press

Therefore, the potential energy of the system is

$$\boldsymbol{U} = \boldsymbol{U}_1 + \boldsymbol{U}_2 + \boldsymbol{U}_f + \boldsymbol{U}_p \tag{56}$$

The generalized force of the system is

$$Q_i = m_2\ddot{q}_i + \left(J_p + J_f\right) / \cos\theta \cdot \ddot{q}_i + (J_1 + J_2)\sin\theta \cdot \ddot{q}_i + m_2 g + m_f g\cos\theta + \frac{4}{3\pi} m_p g \tag{57}$$

Substitute Eqs. (45), (56), and (57) into equation (31) to obtain the dynamic model of the system.

5. Singularity and interference analysis of the mechanism

5.1. Singularity analysis of the mechanism

We determine whether the mechanism is singular using the Jacobian matrix of the series–parallel stable platform. If the mechanism is singular, the following relationship exists

$$|\boldsymbol{J}| = \begin{vmatrix} \frac{1}{l_1'}\left(r^2 s\theta - hrc\theta\right) & 0 \\ -\frac{hrs\theta s\phi}{l_2'} & \frac{1}{l_2'}\left(hrc\theta c\phi + r^2 s\phi\right) \end{vmatrix} = 0 \tag{58}$$

Thus,

$$\frac{1}{l_1' l_2'}\left(r^2 s\theta + hrc\theta\right)\left(hrc\theta c\phi + r^2 s\phi\right) = 0 \tag{59}$$

$$rs\theta - hc\theta = 0 \quad \text{or} \quad hc\theta c\phi + rs\phi = 0 \tag{60}$$

$$\theta = \arctan\left(\frac{h}{r}\right) \quad \text{or} \quad \phi = -\arctan\left(\frac{h}{r}\cos\theta\right) \tag{61}$$

If the mechanism parameters $h = 265$ mm and $r = 100$ mm are known, then $\theta = 69.33°$, because the mechanical limit angle of the mechanism design is pitch angle $\theta = \pm 20.5°$, then no such singular position exists.

For $\phi = -\arctan\left(\frac{h}{r}\cos\theta\right)$, it decreases with the increase in angle θ; when $\theta = \pm 20°$, ϕ becomes the minimum value; therefore, $\phi_{\min} = -\arctan\left(\frac{h}{r}\cos 20°\right) = -68.13°$. Because the mechanical limit angle designed by the mechanism is rolling angle $\phi = \pm 20°$, no such singular position exists. In conclusion, there is no singular position for the mechanism design in the actual operation process.

5.2. Mechanism interference analysis

The possible constraints of mechanism operation include the spherical joint constraint, Hooke joint constraint, rotation pair constraint, middle moving pair length constraint, and interference between connecting members. Let vector n be the direction vector along axis w; we record that the included angle between ball joint Bi and rod Li of the mechanism as η_{i} and the allowable angle of ball joint pair as $\eta_{\max}$; thus,

$$\eta_i = \arccos\frac{n \cdot L_i}{\|n \times L_i\|} \tag{62}$$

The constraint condition for ball joint B_{i} is $\eta_i \le \eta_{max}$.

Similarly, note that the angle of Hooke hinge A_2 is γ, the allowable angle is $\gamma_{\max}$, and the constraint condition is $\gamma_i \le \gamma_{max}$. Because the rotation range of the rotation pair is $[0, 2\pi]$, the constraint of the rotation pair at A1 on the workspace is not considered. The length of the electric push rod is l, and the upper and lower limits of the push rod are $l_{\max} = l_0 + \delta l_{\max}$ and $l_{\min} = l_0 - \delta l_{\max}$, respectively. For a specific pose, the constraint condition of the length of the electric push rod is $l_{\min} \le l \le l_{\max}$.

https://doi.org/10.1017/S0263574725102968 Published online by Cambridge University Press

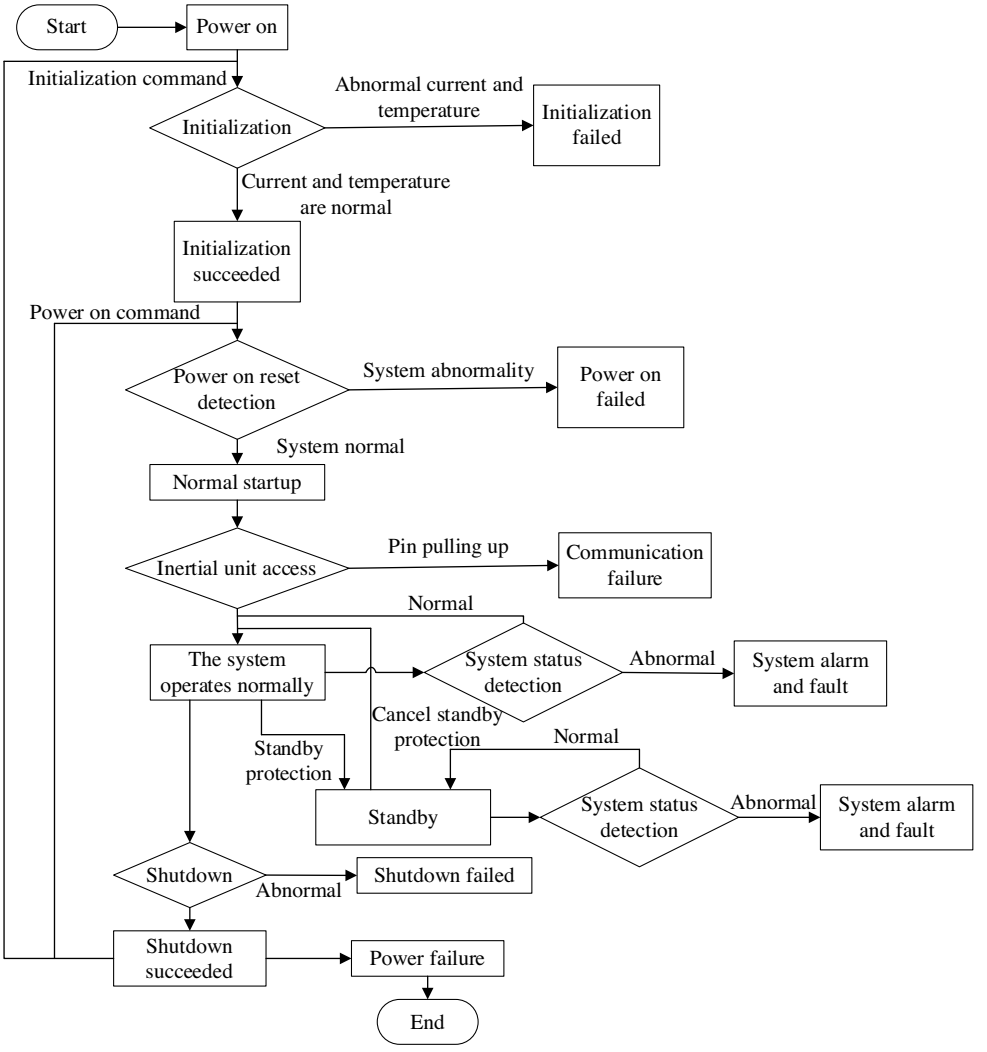


Figure 8. *Working space of the mechanism: (a) isometric view and (b) vertical view.*

During the movement of the mechanism, possible interference exists in the process of the stable platform rotating along the z-axis. The load or moving platform interferes with the box, and the moving platform interferes with the stepping motor. The shortest distance between the rotation center of the recording platform and the box is $r_{1\,\min}$, the shortest distance between the moving platform and the stepping motor is $r_{2\,\min}$, and the condition to avoid interference is $r < [r_{1\,\min}, r_{2\,\min}]_{\min}$. With these constraints, the maximum motion workspace of the mechanism edge is shown in Figure 8. The maximum angle of the two axes is 20°, and the rotation range of the z-axis is [−93°, 93°], which satisfies the actual conditions. The mechanism has no singularity in the workspace and will not interfere with the stepping motor and the box.

6. Design of control system based on state machine

MATLAB/Simulink primarily solves dynamic modeling and simulation problems and completes the design of the controller algorithm. Stateflow can model and simulate event-driven systems based on finite state machine theory, and it can also model and simulate complex logic systems. Simulink and Stateflow were combined to conduct rapid prototyping of the hardware in the loop experiments.

https://doi.org/10.1017/S0263574725102968 Published online by Cambridge University Press

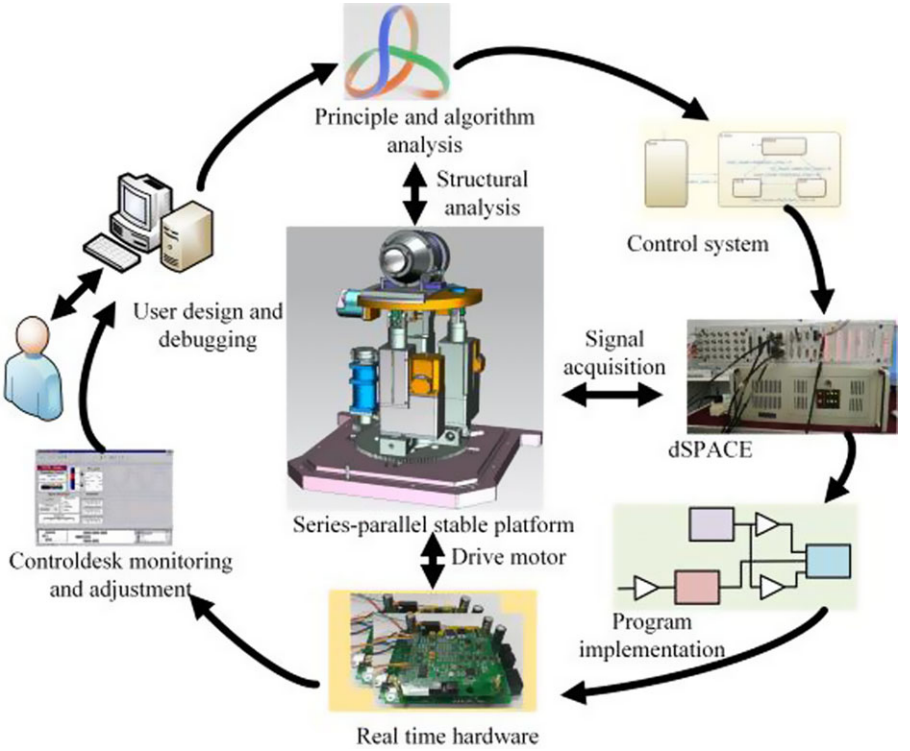


Figure 9. *Workflow chart of the control system.*

6.1. Workflow design of control system

The system workflow during normal operation is shown in Figure 9. The specific workflow is as follows:

6.2. Experimental environment

The application principle of the simulation experiment based on dSPACE of the series–parallel stable platform is shown in Figure 10. The experimental environment primarily included hardware and the software experimental environment. The hardware included a dSPACE system, an industrial personal computer, a servo driver, a series–parallel stable platform, a photoelectric switch, and other hardware. The software environment was primarily composed of the underlying code generated using STM32CubeMX and the controller algorithm and logic system built using Simulink/Stateflow.

6.3. Double closed-loop experiment of position and speed

For a typical input signal $\phi = 6 \sin(2\pi \times 0.25 \times t)$ of the roll motor, the position tracking curve is shown in Figure 11, the speed tracking curve is shown in Figure 12, and the position error curve is shown in Figure 13. The closed-loop system does not have a suppressive effect on high-frequency errors in the transmission chain. For example, tooth profile errors of gears can cause vibrations and noise in the system, resulting in burrs in the error curve. Due to the presence of transmission clearance during commutation, the error curve exhibits a slight lag behind the commutation moment, resulting in spikes.

The analysis of the roll motor was similar to that of the pitch motor. The dynamic tracking accuracy of the system was 1.2′, which satisfied the design index and was reasonable. In conclusion, the single-degree-of-freedom tracking accuracy of the system reached 1.4′, and the system control performance satisfied the performance requirements of practical applications.

https://doi.org/10.1017/S0263574725102968 Published online by Cambridge University Press

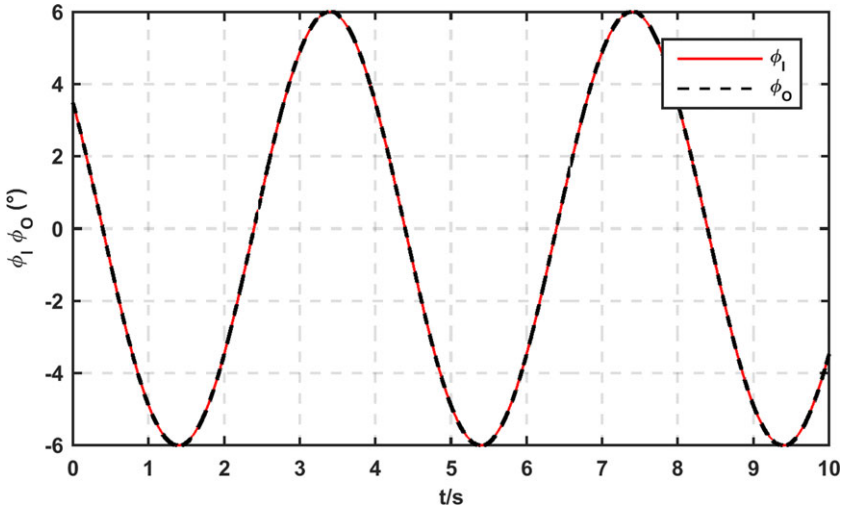


Figure 10. *Principle of dSPACE-based real-time control system.*

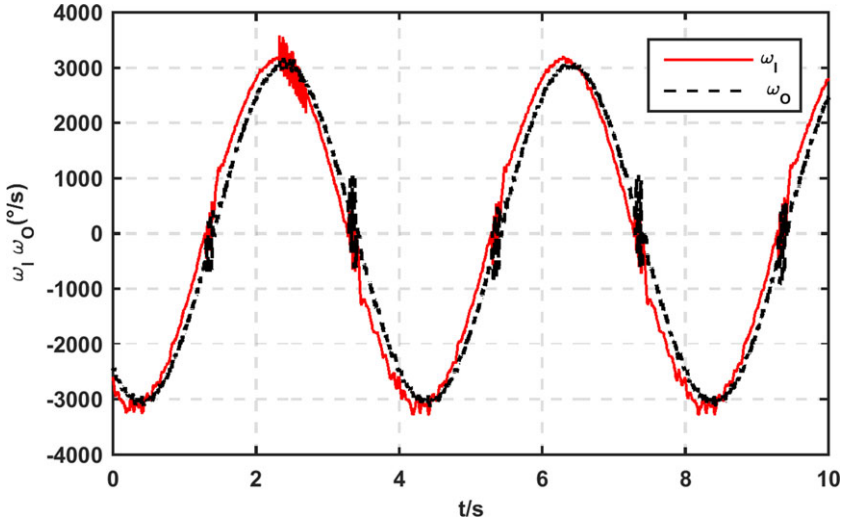


Figure 11. *Roll position tracking.*

6.4. Simulation of mounting carrier given signal experiment

We tested whether the joint response of the series–parallel stable platform satisfies the index. The mounting carrier roll and pitch motion models caused by random signals were input. The pitch position tracking and error curves are shown in Figures 14 and 15, respectively, and the roll position tracking and error curves are shown in Figures 16 and 17, respectively.

Figures 14 and 16 show that the dynamic tracking accuracy of the system was high. Figure 15 shows that the dynamic tracking accuracy of the pitch was 1.5′, and Figure 17 shows that the dynamic tracking accuracy of the roll was 1.2′. The system performance satisfied the performance requirements of practical applications.

6.5. Experimental verification of system comprehensive performance

We installed the series–parallel stable platform on a swing table, and the experimental scenario is shown in Figure 7.

https://doi.org/10.1017/S0263574725102968 Published online by Cambridge University Press

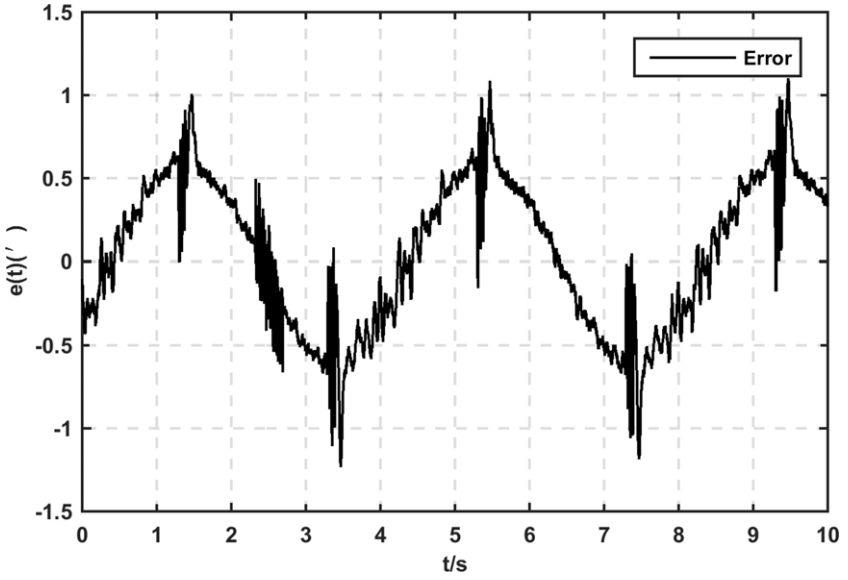


Figure 12. *Roll speed tracking.*

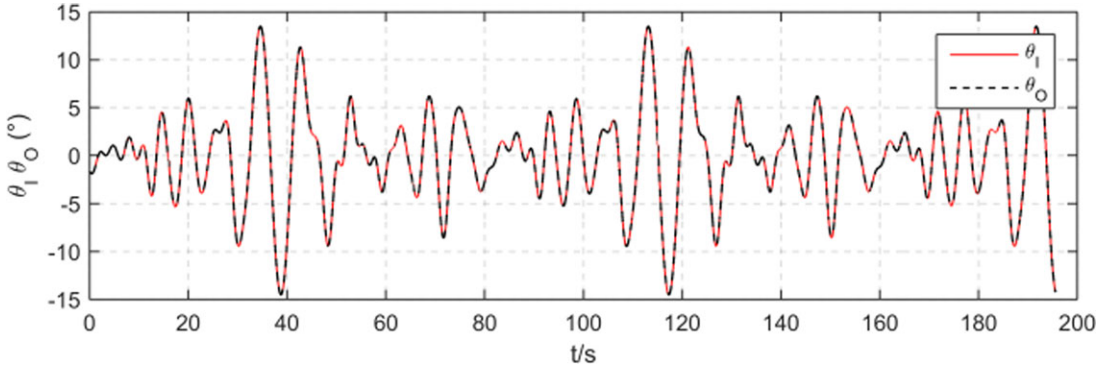


Figure 13. *Roll position error.*

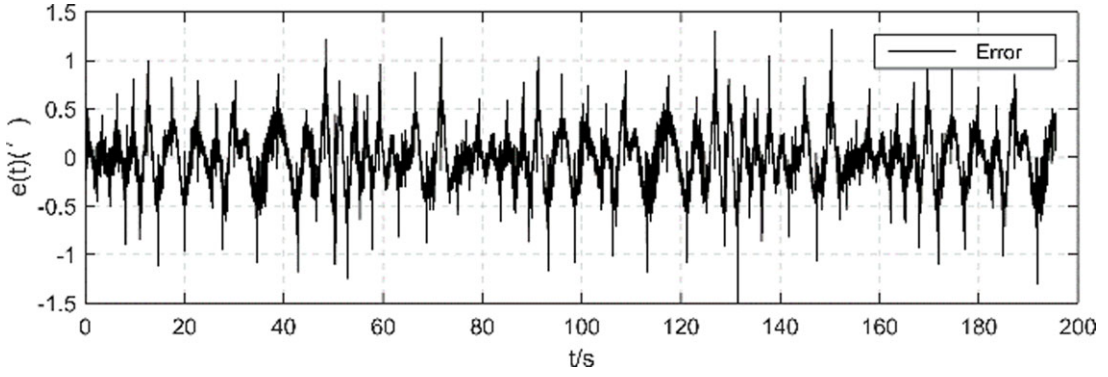


Figure 14. *Pitch position tracking.*

https://doi.org/10.1017/S0263574725102968 Published online by Cambridge University Press

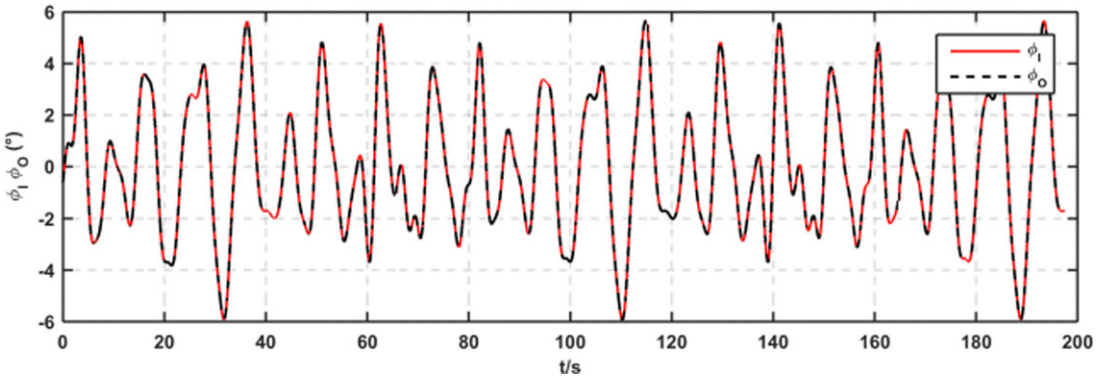


Figure 15. *Pitch position error.*

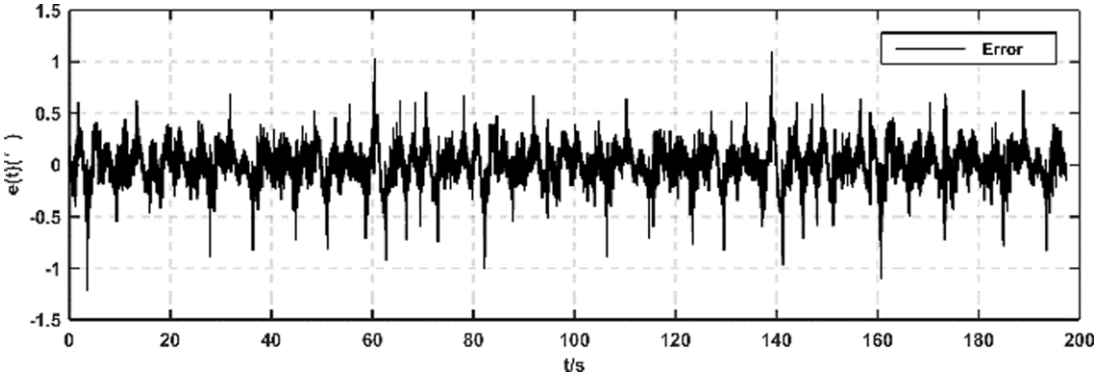


Figure 16. *Roll position tracking.*

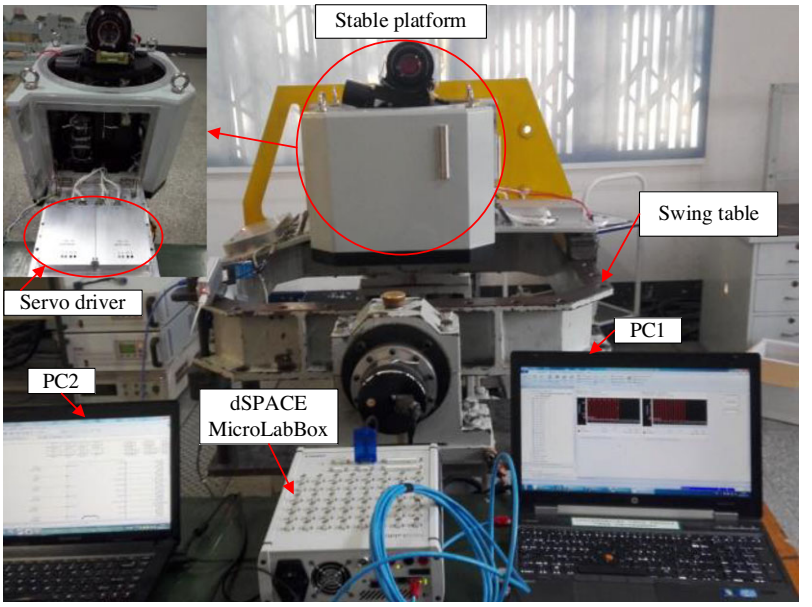


Figure 17. *Roll position error.*

https://doi.org/10.1017/S0263574725102968 Published online by Cambridge University Press

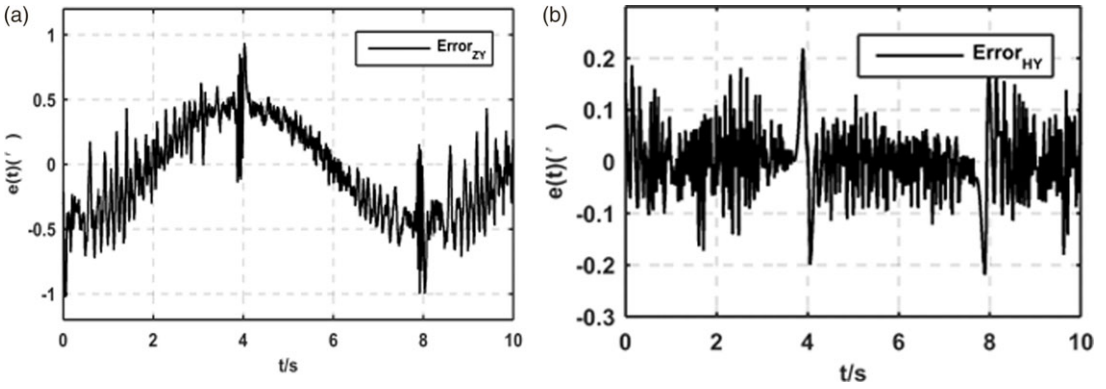


Figure 18. *Azimuth 0° error: (a) pitch and (b) roll.*

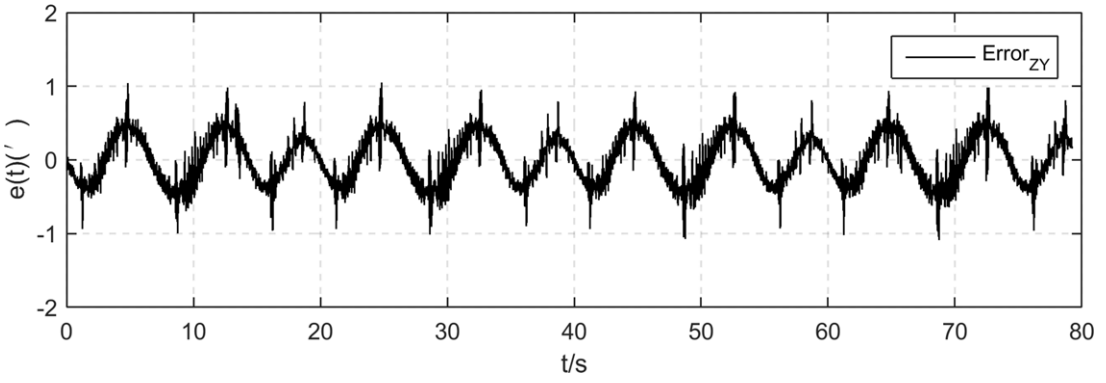


Figure 19. *Pitch error in the azimuth motion.*

The swing platform can achieve different amplitudes and periodic sinusoidal motions. During installation, the pitch direction motion of the stable platform was vertical to the axis of the swing platform, simulating the pitch direction motion of the mounting carrier. By rotating the azimuth at different angles, the movement in two directions was achieved, and the actual application scenario was simulated. In the comprehensive performance, the angle change of the parallel platform was detected by the inertial unit as feedback. The swing platform was started, the amplitude was set to 15°, and the period was set to 8 s. We adjusted the azimuth to 0° and observed the error curves of the pitch and roll directions of the parallel platform, as shown in Figure 18.

When the azimuth angle was 0°, the dynamic accuracy of the pitch mechanism was 1′ (Figure 18(*a*)), and the rolling accuracy was 0.2′ (Figure 18(*b*)). Therefore, the rolling direction was affected to some extent during the movement of the swing table, but the rolling accuracy was very high, which did not affect the stability.

Given the azimuth movement rule as $\gamma = 90\sin(2\pi \times 0.025 \times t)$, we observed the roll and pitch direction error curves of the parallel platform, as shown in Figures 19 and 20.

The mounting carrier pitching signal $\theta = 15\sin(2\pi \times 0.125 \times t)$ was simulated, and the azimuth movement to different angles had a certain impact on the system performance. Figure 19 shows that the dynamic accuracy of the parallel platform pitching direction was 1′, and Figure 20 shows that the dynamic accuracy of the parallel platform rolling direction was 1.3′.

We reinstalled the platform, and the roll direction movement of the stable platform was perpendicular to the axis of the swing platform, simulating the roll direction movement of the mounting carrier. The movement of two degrees of freedom was achieved using different angles rotating through the azimuth angle. The swing platform was started, the amplitude was set as 6° and the period as 4 s, the azimuth

https://doi.org/10.1017/S0263574725102968 Published online by Cambridge University Press

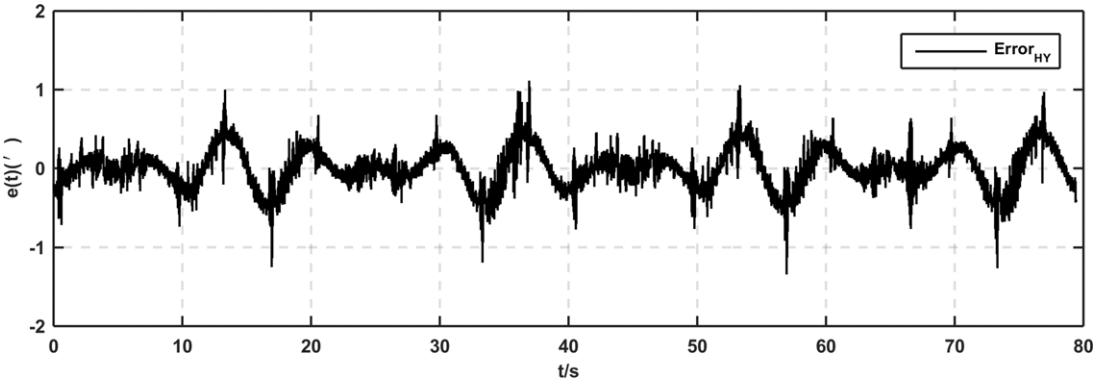


Figure 20. *Roll error in the azimuth motion.*

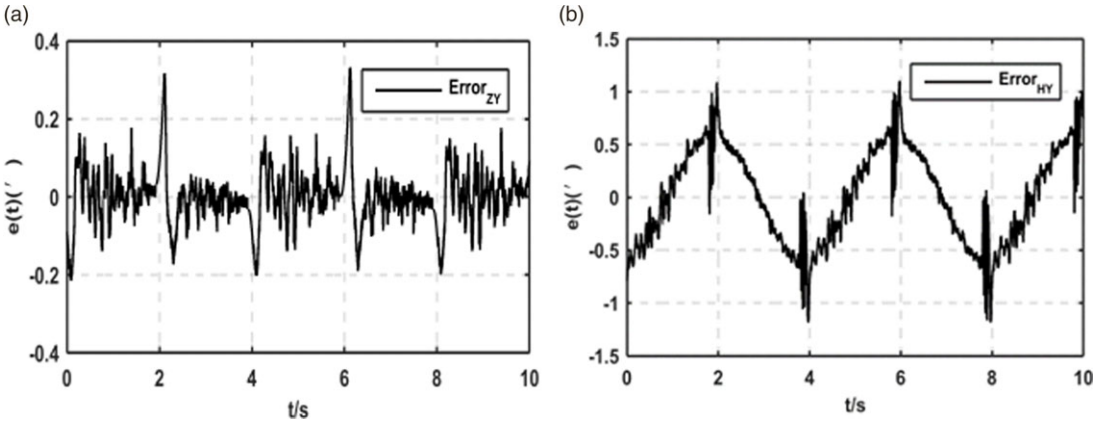


Figure 21. *Azimuth 0° error: (a) pitch and (b) roll.*

angle was adjusted to 0°, and the error curves of the parallel platform in the pitch and roll directions were observed, as shown in Figure 21.

When the azimuth angle was 0°, Figure 21(*a*) shows that the dynamic accuracy of the pitch mechanism was 0.3′, and Figure 21(*b*) shows that the rolling accuracy was 1.1′. Therefore, the motion of the swing platform had a certain impact on the pitch direction, but the pitch accuracy was very high, which did not affect the stability.

Given the azimuth movement rule as $\gamma = 90\sin(2\pi \times 0.025 \times t)$, we observed the roll direction and pitch direction error curves of the parallel platform, as shown in Figures 22 and 23.

The mounting carrier roll signal $\phi = 6\sin(2\pi \times 0.25 \times t)$ was simulated, and the azimuth movement to different angles had a certain impact on the system performance. Figure 22 shows that the dynamic accuracy of the pitch was 1.5′, and Figure 23 shows that the dynamic accuracy of the roll was 1.5′.

In conclusion, the dynamic tracking accuracy of the series–parallel stable platform reached 1.5′, which satisfied the performance requirements of the system in practical application.

7. Conclusions

1. In this paper, a novel series–parallel three-degree-of-freedom stable platform is designed, and it combines an azimuth mechanism with a two-degree-of-freedom parallel platform. The mechanism scheme and control system are designed. The kinematics and dynamics models of the series–parallel three-degree-of-freedom stable platform are established. A Simulink simulation analysis was conducted to verify the feasibility of the mechanism.

https://doi.org/10.1017/S0263574725102968 Published online by Cambridge University Press

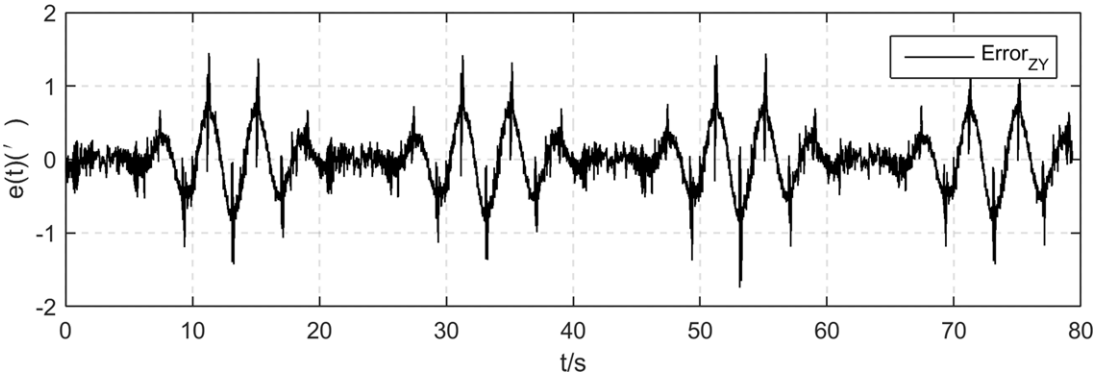


Figure 22. *Pitch error in the azimuth motion.*

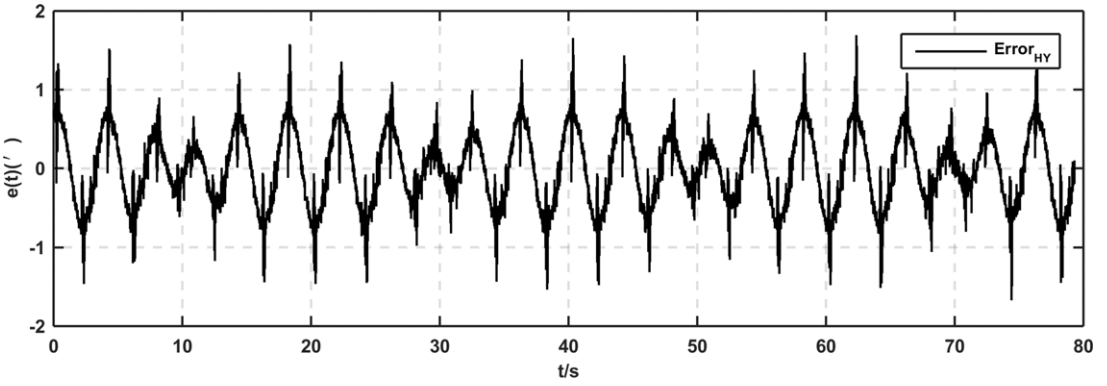


Figure 23. *Roll error in the azimuth motion.*

2. The control system based on the state machine was designed. Based on dSPACE, a semi-physical simulation platform was built to conduct experimental research on the prototype of the series–parallel stable platform, which verified the feasibility of the control system, and the control performance satisfied the indicators.
3. The stable platform was installed on a swing platform to simulate the motion of the mounting carrier under the random swing. When the azimuth angle moved, it operated smoothly, and the system tracking accuracy was 1.5′. This verified that the design of the control system is reasonable and satisfies the performance requirements of practical applications.

In the future, sensor data fusion technology will be applied to detect sensor faults, analyze the impact of gear transmission noise on system performance, and further enhance system performance.

8. Required declarations

Author contribution. Xinlei Xiao, Da Song, Lei Lu, and Lixun Zhang conceived and designed the study. Da Song and Feng Xue conducted data gathering. Gang Li performed statistical analyses. Xinlei Xiao and Da Song wrote the article.

Financial support. This work was supported by the Natural Science Foundation of Jilin Province (Grant No. YDZJ202301ZYTS272).

Competing interests. The authors declare no conflicts of interest exist.

Ethical approval. Not applicable.

https://doi.org/10.1017/S0263574725102968 Published online by Cambridge University Press

References

[1] S. K. Mishra and C. S. Kumar, "Compliance modeling of a full 6-DOF series–parallel flexure-based Stewart platform-like micromanipulator," *Robotica* **40**(10), 3435–3462 (2022).

[2] C. Tian and D. Zhang, "A new family of generalized parallel manipulators with configurable moving platforms," *Mech. Mach. Theory* **153**, 103997 (2020).

[3] G. Wang and L. Wang, "Coupling relationship of the non-ideal parallel mechanism using modified Craig-Bampton method," *Mech. Syst. Signal Process.* **141**, 1064711–10647128 (2020).

[4] M. Slavutin, A. Sheffer, O. Shai and Y. Reich, "A complete geometric singular characterization of the 6/6 Stewart platform," *J. Mech. Robot. ASME* **10**(4), 041012–1–10 (2018).

[5] R. Wang, S. Li and Y. Li, "A suspended cable-driven parallel robot with articulated reconfigurable moving platform for schönflies motions," *IEEE/ASME Trans. Mechatron.* **27**(6), 5173–5184 (2022).

[6] G. Zhang, J. Guo, Y. Hou and D. Zeng, "Analysis of the PU-2UPS antenna parallel mechanism," *J. Mech. Sci. Technol.* **35**(2), 717–728 (2021).

[7] R. S. Geronel, G. C.êa de Oliveira, G. K. Rodrigues and M. M. da Silva, "Active vibration control of a flexible parallel manipulator 3RRR," *Robotica* **43**(6), 2081–2099 (2025).

[8] S. Peng, L. Du, L. Che and Z. Jin, "Dimensional multi-objective optimization design for 2RPU-RPS parallel mechanism," *Robotica* **43**(3), 1087–1109 (2025).

[9] J. Zhang, Y. Song and D. Liang, "Mathematical modeling and dynamic characteristic analysis of a novel parallel tracking mechanism for inter-satellite link antenna," *Appl. Math. Model.* **93**, 618–643 (2021).

[10] Y. Song, G. Dong and T. Sun, "Elasto-dynamic analysis of a novel 2-DoF rotational parallel mechanism with an articulated travelling platform," *Meccanica* **51**(7), 1547–1557 (2016).

[11] Z. Chong, F. Xie, X. Liu and J. Wang, "Evaluation of dynamic isotropy and coupling acceleration capacity for a parallel manipulator with mixed DoFs," *Mech. Mach. Theory* **163**(6), 104382 (2021).

[12] W. Haouas, R. Dahmouche, N. L. Fort-Piat and G. J. Laurent, "A new seven degrees-of-freedom parallel robot with a foldable platform," *J. Mech. Robo.: Trans. ASME* **4**, 1–15 (2018).

[13] Z. Lin, W. Dong, S. Liu, X. Sheng and X. Zhu, "An efficient egocentric regulator for continuous targeting problems of the underactuated quadrotor," *IEEE/ASME Trans. Mechatron.* **28**(1), 116–127 (2023).

[14] P. Shao, Z. Wang, S. Yang and Z. Liu, "Dynamic modeling of a two-DoF rotational parallel robot with changeable rotational axes," *Mech. Mach. Theory* **131**, 318–335 (2019).

[15] F. Xie, X.-J. Liu and J. Wang, "A 3-DOF parallel manufacturing module and its kinematic optimization," *Robot. Comput. Int. Manuf.* **28**(3), 334–343 (2012).

[16] T. Sun, D. Liang and Y. Song, "Singular-perturbation-based nonlinear hybrid control of redundant parallel robot," *IEEE Trans. Ind. Electron.* **65**(4), 3326–3336 (2018).

[17] S. Tao, Y. Song, D. Gang, B. Lian and J. Liu, "Optimal design of a parallel mechanism with three rotational degrees of freedom," *Robot. Comput. Int. Manuf.* **28**(4), 500–508 (2012).

[18] M. Slavutin, A. Sheffer, Y. Reich and O. Shai, "A novel criterion for singularity analysis of parallel mechanisms," *Mech. Mach. Theory* **137**, 459–475 (2019).

[19] D. Xu, S. Gou, X. Jin, F. Zhao and Y. Fang, "Design and analysis of a novel class of hybrid parallel manipulators with $3+3$ degrees of freedom and remotely operated grippers," *Mech. Mach. Theory* **212**, 106073 (2025).

[20] X. Liu and J. Kim, "A new spatial three-DoF parallel manipulator with high rotational capability," *IEEE/ASME Trans. Mechatron.* **10**(5), 502–512 (2005).

[21] L. Yu, B. Bl, C. Wx and B. Xw, "A method for measuring the inertia properties of a rigid body using 3-URU parallel mechanism," *Mech. Syst. Signal Process.* **123**, 174–191 (2019).

[22] X. Liu, J. Mao, J. Yang, S. Li and K. Yang, "Robust predictive visual servoing control for an inertially stabilized platform with uncertain kinematics," *ISA Trans.* **114**, 347–358 (2021).

[23] X. Zhou, H. Zhang and R. Yu, "Decoupling control for two-axis inertially stabilized platform based on an inverse system and internal model control," *Mechatronics* **24**(8), 1203–1213 (2014).

[24] B. Hu, Y. Shi, L. Xu and P. Bai, "Reconsideration of terminal constraint/mobility and kinematics of 5-DOF hybrid manipulators formed by one 2R1T PM and one RR SM," *Mech. Mach. Theory* **149**, 103837 (2020).

[25] G. A. Jaime, "Enhancing the originality of the Stewart platform through its kinematic analyses," *Proc. Inst. Mech. Eng. Pt. C J. Mechan. Eng. Sci.* **226**(12), 3013–3025 (2013).

[26] S. H. Lee, J. B. Song, W. C. Choi and D. Hong, "Position control of a Stewart platform using inverse dynamics control with approximate dynamics," *Mechatronics* **13**(6), 605–619 (2003).

[27] T. Ono, R. Eto, J. Yamakawa and H. "Murakami., "Analysis and control of a Stewart platform as base motion compensators - Part I: Kinematics using moving frames," *Nonlinear Dynam.* **107**, 51–76 (2021).

[28] H. Yun, L. Liu, Q. Li, W. Li and L. Tang, "Development of an isotropic Stewart platform for telescope secondary mirror," *Mech. Syst. Signal Process.* **127**, 328–344 (2019).

[29] S. Liu, G. Peng and H. Gao, "Dynamic modeling and terminal sliding mode control of a 3-DOF redundantly actuated parallel platform," *Mechatronics* **60**, 26–33 (2019).

[30] Z. Hurak and M. Rezac, "Image-based pointing and tracking for inertially stabilized airborne camera platform," *IEEE Trans. Contr. Syst. Tech.* **20**(5), 1146–1159 (2012).

https://doi.org/10.1017/S0263574725102968 Published online by Cambridge University Press

[31] F. Königseder, W. Kemmetmüller and A. Kugi, "Attitude control strategy for a camera stabilization platform," *Mechatronics* **46**, 60–69 (2017).
[32] D. Ke, S. Cong, D. Kong and H. Shen, "Discrete-time direct model reference adaptive control application in a high-precision inertially stabilized platform," *IEEE Trans. Ind. Electron.* **66**(1), 358–367 (2018).
[33] J. Wu, G. Yu, Y. Gao and L. Wang, "Mechatronics modeling and vibration analysis of a 2-DOF parallel manipulator in a 5-DOF hybrid machine tool," *Mech. Mach. Theory* **121**, 430–445 (2018).

Cite this article: X. Xiao, D. Song, L. Lu, G. Li, F. Xue and L. Zhang (2025). "Modeling analysis and signal tracking experiment of a novel series–parallel stable platform system", Robotica **43**, 4476–4497. https://doi.org/10.1017/S0263574725102968

https://doi.org/10.1017/S0263574725102968 Published online by Cambridge University Press